

The Relation between Dendritic Geometry, Electrical Excitability, and Axonal Projections of L2/3 Interneurons in Rat Barrel Cortex

Moritz Helmstaedter¹, Bert Sakmann¹ and Dirk Feldmeyer^{2,3}

¹Department of Cell Physiology, Max-Planck Institute for Medical Research, Jahnstraße 29, D-69120 Heidelberg, Germany, ²Research Centre Jülich, Institute for Neuroscience and Biophysics, INB-3 Medicine, Leo-Brandt-Strasse, D-52425 Jülich, Germany and ³Department of Psychiatry and Psychotherapy, RWTH Aachen University, Pauwelsstrasse 30, D-52074 Aachen, Germany

Interneurons in layer 2/3 (L2/3) of the somatosensory cortex show 4 types of axonal projection patterns with reference to the laminae and borders of columns in rat barrel cortex (Helmstaedter et al. 2008a). Here, we analyzed the dendritic geometry and electrical excitability of these interneurons. First, dendritic polarity, measured based on the insertion points of primary dendrites on the soma surface, yielded a continuous one-dimensional measure without a clustering of dendritic polarity types. Secondly, we analyzed polar and vertical distributions of dendritic length. A cluster analysis allowed the definition of 7 types of dendritic arborization. Thirdly, when dendritic polarity was related to the intrinsic electrical excitability we found that the ratio of frequency adaptation in trains of action potentials (APs) evoked by current injection was correlated with the number of primary dendrites. Numerical simulations of spiking patterns in L2/3 interneurons suggested that the number of primary dendrites could account for up to 50% of this correlation. Fourthly, dendritic arborization was not correlated with axonal projection, and axonal projection types could not be predicted by electrical excitability parameters. We conclude that 1) dendritic polarity is correlated to intrinsic electrical excitability, and 2) the axonal projection pattern represents an independent classifier of interneurons.

Keywords: barrel cortex, cluster analysis, dendrites, electrical excitability, GABAergic interneuron, layer 2/3, simulation

Introduction

Approximately 10–20% of neocortical neurons are nonpyramidal, mostly gamma-aminobutyric acidergic (GABAergic) interneurons (Beaulieu 1993). The shape of the soma, dendrite and axon geometry of nonpyramidal neurons is highly diverse, and numerous classifications have been suggested based on this diversity (Ramón y Cajal 1904; Lorente de No 1938; Szentagothai 1973; Jones 1975; Feldman and Peters 1978; Gibson et al. 1999; Cauli et al. 2000; Gupta et al. 2000). In several studies electrical membrane properties of nonpyramidal neurons were characterized, and a matching of electrical and morphological parameters was attempted (McCormick et al. 1985; Connors and Gutnick 1990; Foehring et al. 1991; Gupta et al. 2000; Krimer et al. 2005; Zaitsev et al. 2005). In addition, immunohistochemical markers have been suggested to define classes of nonpyramidal neurons (Cauli et al. 1997; Gonchar and Burkhalter 1997; Kawaguchi and Kubota 1997; Miyoshi et al. 2007; Gonchar et al. 2008).

The concomitant measurement of all of the suggested classification parameters in a single experiment is a major methodological challenge. Consequently, subsets of parameters (typically shape of the soma or AP firing pattern) were used to

preselect populations of cells at the beginning of an experiment (e.g., Gibson et al. 1999; Beierlein et al. 2000; Cauli et al. 2000; Wang et al. 2002; Karube et al. 2004; Toledo-Rodriguez et al. 2005). It is however not clear a priori, whether subsets of dendritic, electrical or axonal parameters are in fact valid surrogates for the detailed classifications that were originally based on a much larger set of classifying parameters (Ramón y Cajal 1904; Somogyi et al. 1983; Tamás et al. 1998).

Here, geometries of dendritic arbors, passive and active membrane properties, and axonal projection patterns (cf. Helmstaedter et al. 2008a) were evaluated in a sample of 64 interneurons in layer 2/3 of rat somatosensory cortex in the fourth postnatal week (P20–29). Neurons were not preselected based on DIC image or firing patterns (cf. Methods). The analysis was pursued as follows:

1. Dendritic geometry was quantified using (a) an analytical one-dimensional measure of dendritic polarity and (b) a categorical scale of dendritic types derived by a cluster analysis (CA) based on the dendritic length density distribution. The 2 measures of dendritic geometry were highly correlated.
2. Dendritic polarity was related to electrical excitability. Here, strong correlations were found. Numerical simulations of the AP firing patterns were used to separate any possible causal effect of dendrite geometry from the contribution of membrane conductances.
3. Canonical correlation analysis was then used to identify whether dendritic geometry or electrical excitability could predict the type of axonal projection. This was however not the case: thus axonal projections represent an independent classifier of interneurons.

Methods

Preparation, Solutions

All experimental procedures were performed according to the animal welfare guidelines of the Max-Planck Society. Wistar rats (20–29 days old) were anesthetized with isoflurane and decapitated, and slices of somatosensory cortex were cut in cold extracellular solution using a vibrating microslicer (DTK-1000; Dosaka, Kyoto, Japan). Slices were cut at 350- μ m thickness in a thalamocortical plane (Agmon and Connors 1991) at an angle of 50° to the interhemispheric sulcus. Slices were incubated at room temperature (22–24°C) in an extracellular solution containing 4 mM MgCl₂/1 mM CaCl₂ to reduce synaptic activity. Slices were continuously superfused with an extracellular solution containing (in mM): 125 NaCl, 2.5 KCl, 25 glucose, 25 NaHCO₃, 1.25 NaH₂PO₄, 2 CaCl₂, and 1 MgCl₂ (bubbled with 95% O₂ and 5% CO₂). The pipette (intracellular) solution contained (in mM): 105 K-gluconate, 30 KCl, 10 HEPES, 10 phosphocreatine, 4 ATPMg, and 0.3 GTP (adjusted to pH 7.3 with KOH); the osmolarity of the solution

was 300 mOsm Biocytin (Sigma, Munich, Germany) at a concentration of 3–6 mg/mL was added to the pipette solution, and cells were filled during 1–2 h of recording, with the exception of neurons that were later used for immunohistochemical analysis (Supplementary Material).

Identification of Barrels and Neurons

Slices were placed in the recording chamber and inspected with a 2.5×/0.075 numerical aperture (NA) Plan objective using bright-field illumination. Barrels were identified as evenly spaced, light “hollows” separated by narrow dark stripes (Agmon and Connors 1991; Feldmeyer et al. 1999) and photographed using a frame-grabber for later analysis. Interneurons were searched in layer 2/3 above barrels of $250 \pm 70 \mu\text{m}$ width ($n = 64$) using a water immersion objective 40×/0.80 NA and infrared differential interference contrast microscopy (Dodt and Zieglansberger 1990; Stuart et al. 1993). Somata of neurons in layer 2/3 were selected for recording if a single apical dendrite was not visible. This was the sole criterion for the a priori selection of interneurons. After recording, the pipettes were positioned above the slice at the position of the recorded cells, and the barrel pattern was again photographed using bright-field illumination.

Histological Procedures

After recording, slices were fixed at 4°C for at least 24 h in 100 mM phosphate buffer, pH 7.4, containing either 4% paraformaldehyde or 1% paraformaldehyde and 2.5% glutaraldehyde. Slices containing biocytin-filled neurons were processed using a modified protocol described previously (Lübke et al. 2000). Slices were incubated in 0.1% Triton X-100 solution containing avidin-biotinylated horseradish peroxidase (ABC-Elite; Camon, Wiesbaden, Germany); subsequently, they were reacted using 3,3-diaminobenzidine as a chromogen under visual control until the dendritic and axonal arborizations were clearly visible. To enhance staining contrast, slices were occasionally postfixed in 0.5% OsO₄ (30–45 min). Slices were then mounted on slides, embedded in Moviol (Clariant, Sulzbach, Germany), and enclosed with a thin coverslip (see below).

Reconstruction of Neuronal Morphologies

Subsequently, neurons were reconstructed with the aid of NeuroLucida software (MicroBright-Field, Colchester, VT) using an Olympus Optical (Hamburg, Germany) BX50 microscope at a final magnification of 1000× (using a 100×, 1.25 NA objective). The reconstructions provided the basis for the quantitative morphological analysis (see below). The soma was reconstructed by drawing a contour along its largest circumference. To do so, the soma circumference was first observed in the plane of the slice (xy -plane). Then, at each location along the largest soma circumference in the xy -plane, the focus was set such that the soma border appeared most clear. This focal depth was then recorded as the z -coordinate of this point. In the *Rembrandt II* software, the resulting contour line was sampled in 1- μm steps along the y -axis. The soma midline was determined as average x - and z -coordinate of the circumference contour for each y -segment. From this data, the soma was converted to a sequence of cylindrical pieces with midpoints along the soma midline, radius of half the distance between the contour lines in each y -segment and of 1- μm thickness along the y -axis. This procedure yielded a volume approximation of the soma that was rotationally symmetric along the midline of the soma. Given the sampling precision and optical limitations, we estimate the spatial precision of the soma reconstruction to be on the order of 1–2 μm .

The pial surface of the slice was also reconstructed. The reconstruction was rotated in the plane of the slice such that the pial surface above the reconstructed neuron was horizontally aligned. Thus, the x -axis of the reconstruction was parallel to the pia in the plane of the slice, the y -axis perpendicular to the pia in the plane of the slice.

Reconstructions were used for quantitative analysis of axonal projections, if the axonal arbor had a path length of at least 4 mm (cf. Helmstaedter et al. 2008a). The average axonal path length however was much higher ($20 \pm 11 \text{ mm}$, Helmstaedter et al. 2008a). Due to the geometry of the in vitro slice preparation (slice thickness: 350 μm), longer-range (>1 mm) lateral axonal projections could potentially be lost during sectioning. We chose a quantitative criterion

(total axonal path length) for judgment of slicing artifacts to prevent an observer bias introduced by qualitative exclusion criteria. Dendrites were analyzed if the dendritic arbor was not cut by the sectioning procedure.

Tissue Shrinkage

To estimate shrinkage in the xy -plane, we compared the distance between the soma and the pia, or the 2 somata of paired recordings before fixation (using the bright-field image taken during the experiment) and after fixation (using the computer reconstruction). Shrinkage in the xy -plane was $11 \pm 6\%$ (range 0–25%). A recent study (Egger et al. 2008) found nonlinear shrinkage in the z -direction that was strongest at the slice surface (presumably due to adhesive forces between the tissue and the glass coverslip) and amounted to approximately 50% in the z -direction. To reduce shrinkage in the z -direction, we used very thin glass coverslips (0.04–0.06 mm thickness, Menzel Thermo Fisher Scientific, Braunschweig, Germany). For some samples, the coverslip was removed before reconstruction. Dendritic polarity is generally assumed to occur along an axis perpendicular to the cortical surface (here: the y -axis; for an overview, see e.g., Jones 1975). Thus, for measures of dendritic polarity, shrinkage along the z -axis is of less relevance. The systematic underestimation of axonal or dendritic path length by shrinkage was estimated to be up to 25% (assuming isotropic dendritic distributions and shrinkage of 15% in xy , and 50% in z). We did not use shrinkage correction for the following analyses.

Dendritic Polarity

The reconstruction of the neuronal morphology (ASC file format as provided by the NeuroLucida software) was then read-in by the custom-made software *Rembrandt II* (written in IGOR PRO, Lake Oswego, OR). The insertion points of the primary dendrites on the approximated surface of the soma were determined as the intersection of the somatic surface and the linear interpolation between the first reconstructed point of the dendrite and the soma center. The calculation of the polarity index is described in the Results and further detailed in the Supplementary Material (Supplementary Figs 1 and 2). We use the term “dendritic polarity” for reference to the polarity of primary dendrites, and the term “dendritic geometry” to summarize geometrical properties of the dendrites (including the dendritic polarity index, dendritic density distributions, length per primary dendrite, total dendritic length, and the number of primary dendrites).

Dendritic Density Distributions

For the analysis of dendritic density distributions, dendritic reconstructions were converted to the NEURON format (.hoc) using the custom-made parser *Rembrandt II*. In NEURON (Hines and Carnevale 1997), 3d arc length of dendritic segments were measured and summed in either radial or Cartesian bins in the plane of the slice.

The final dendritic feature vector consisted of 1) the angular dendritic length distribution for the complete dendritic tree (36 parameters, bin size 10°), 2) the angular dendritic length distribution within a sphere of 30 μm radius around the soma (36 parameters, bin size 10°), 3) the angular dependence of the maximum dendritic extent from the soma (12 parameters, bin size 30°, weight factor 2), and 4) the distribution of dendritic length along the y -axis (17 parameters, bin size 50 μm). The angular length distributions were aligned such that the maximum was at 0° allowing a maximal rotation of $\pm 20^\circ$. The cluster analyses were made on this 101-dimensional feature vector in MATLAB (Mathworks, Natick, MA) using Ward’s method (Ward 1963) for linkage and Euclidean distances. For an independent criterion for cluster cutoff, 4 L2/3 pyramidal neurons were included in the analysis (reconstructions are shown in the Supplementary Material). The criterion for cluster cutoff distance was that no pyramidal neuron should be linked to an interneuron (this defined the upper boundary for cluster cutoff linkage distance), and that pyramidal neurons should be linked in one cluster (this defined the lower boundary for cluster cutoff linkage distance). The correlation analyses presented in this study did not depend on the choice of cluster cutoff distance within these boundaries.

Canonical Correlations

To test the predictive power of parameter sets, multidimensional multivariate correlations were calculated using SPSS for Windows 14.0 (SPSS, Inc, Chicago, IL): The multivariate tests of significance for within cells regression of 4 dendritic parameters with 2 axonal parameters (Fig. 10C) were at significance levels >0.11 for all used test metrics (Pillais, Hotellings, Wilks Lambda). For the test of 5 electrophysiological parameters with 2 axonal parameters (Fig. 11D), significance levels were >0.14 . For the test of the 9 combined electrophysiological and dendritic parameters with 2 axonal parameters (Fig. 12), significance levels were >0.11 .

Electrical Excitability Parameters

We recorded basic parameters describing the electrical excitability of the neurons that have been typically used in the literature. A sequence of depolarizing 500-ms-long rectangular current pulses of varying amplitudes was applied, and the action potential (AP) sequences were recorded. For analysis, the trace with an initial inter-AP-interval that was closest to 10 ms (100 Hz) was used (Beierlein et al. 2003). First, the intervals between subsequent APs were measured. The inverse ("AP frequencies") was then fitted to a monoexponential function. The ratio of the offset of this function to its initial value was recorded as the "AP frequency adaptation ratio" at 100 Hz. Then, the minimum voltage of the AP-after hyperpolarization was measured as the minimum voltage between 2 AP peaks. A monoexponential function was fitted to the after hyperpolarization (AHP) minimum voltages within one AP train, and the ratio of the offset to the initial value was recorded as "AHP-adaptation ratio." The half width of all APs in the 100-Hz trace were determined and averaged. Half width was measured as the AP width at half-maximal amplitude. Half-maximal amplitude was measured as half the difference between the median membrane voltage during the current pulse and the AP peak voltage. Finally, the apparent AP threshold was determined as the median voltage during the depolarizing current pulse, averaged for the last sweep with no AP firing and the first sweep with at least one AP firing.

Nomenclature

The description of morphological and physiological features in this manuscript made—where applicable—use of the nomenclature recently suggested by the Petilla Convention (Ascoli et al. 2008).

Sample Size

In total, 64 L2/3 interneurons were analyzed. Electrical properties were analyzed for all 64 interneurons with the exception of AP threshold potential ($n = 56$). The dendritic arbor of 7 of 64 interneurons did not show sufficient staining for quantitative analysis, thus dendritic and electrical properties were analyzed simultaneously for 57 interneurons (including AP threshold potential: $n = 49$ neurons). The axonal arbor of 51 interneurons met the criteria for completeness of axonal reconstruction as described above; thus axonal and electrical properties were analyzed simultaneously for 51 interneurons. These 51 interneurons were also analyzed in the previous paper (Helmstaedter et al. 2008a). Axonal, dendritic and electrical properties could be analyzed simultaneously for 39 interneurons. These 39 interneurons also were used for the CA presented in the following study (Helmstaedter et al. 2008b). The original reconstructions are shown in the Supplementary material and are also provided online in the .asc format: <http://www.mpimf-heidelberg.mpg.de/~mhelmsta/interneurons>.

Results

Dendritic Polarity

We devised a quantitative measure of "dendritic polarity" as a function of the distribution of the primary dendrite insertion points on the surface of the soma. Figure 1 shows 2 examples of dendritic geometries, which are designated "multipolar" (Fig. 1A) and "bipolar" (Fig. 1E). Surface maps of the soma of the 2 interneurons are shown in Figure 1B,F. The origins of

the primary dendrites are marked on the soma surface maps (Fig. 1B,F, crosses). Cluster analyses (CAs) were applied to the x, y and z-coordinates of the dendrite origins. Figure 1A shows a neuron with eleven primary dendrites. Their origins are almost homogeneously distributed on the soma surface (Fig. 1B). The CA on dendrite insertion points yielded the cluster linkage plot displayed in Figure 1C. The maximum linkage distance was normalized to the maximum of the soma diameters d_x, d_y (Fig. 1B). The smaller linkage distances were normalized to the minimum of the 2 soma diameters. Figure 1D shows the resulting distribution of normalized cluster distances for the neuron in Figure 1A. The largest linkage distance is only 66% of the larger soma diameter. The second largest linkage distance is 71% of the smaller soma diameter; the third and fourth linkage distances are 50% and 40% of the smaller soma diameter. This geometry contrasts with the geometry of the "bipolar" cell shown in Figure 1E-H. Figure 1G shows the CA linkage plot for the dendrite origins of the neuron in Figure 1E. Two dendrites (dend01, dend02) are clustered at a small linkage distance of 1.4 μm (linkage distances are defined as spatial Euclidean distances). This "cluster" of 2 dendrites is linked to the remaining third dendrite (dend03) at a much larger linkage distance of 10.3 μm . Figure 1H shows the 2 normalized cluster distances for the neuron in Figure 1E. The maximum linkage distance spans 80% of the maximum soma diameter, the second linkage distance is low ($<20\%$ of the minimum soma diameter).

The first 3 cluster distances (d_1, d_2, d_3) and the number of dendrites (n) were used as independent variables for a ratio-metric scale of dendrite polarity. The highest linkage distance (d_1) was normalized to the larger soma diameter, and the second and third linkage distance (d_2, d_3) were normalized to the smaller soma diameter. Polarity was defined as a function of these 4 parameters (for details see Methods and Supplementary Material). The interneurons shown in Figure 1 had a dendrite polarity index of 6.1 (Fig. 1A) and 2.3 (Fig. 1E), respectively. This dendritic polarity index was then used to investigate possible functional consequences of "bipolarity" or "multipolarity" of interneurons. Figure 2 shows the relation between dendritic polarity and the number of primary dendrites ($n = 57$). Dendritic polarity was highly correlated to the number of primary dendrites ($r = 0.91, p < 1e-6$).

Dendritic Density Distributions

We next investigated the spatial distribution of dendritic length of L2/3 interneurons in 2D and 3D. To detect the polarity of dendritic trees we computed polar histograms of dendritic path lengths both for the entire dendritic tree (Fig. 3B) and for the part of the dendritic tree that was located within a sphere of 30- μm radius from the soma center (Fig. 3C). Figure 3D shows the polar distribution of the maximal distance of dendrites from the soma center. To measure dendritic arborizations with tufts we also quantified the dendritic length distribution along an axis perpendicular to the brain surface in the plane of the slice (shown in Fig. 3E). These parameters were used to detect clusters of types of dendritic geometry. Figure 4A shows the linkage plot of a CA (Ward's Method; Ward 1963). Four L2/3 pyramidal neurons were included in the analysis, and the cutoff linkage distance was chosen such that pyramidal neurons were not linked to interneurons (dashed line in Fig. 4A, for a detailed account of the cutoff definition see Methods; reconstruction are shown in the Suppl. Material). This analysis yielded 7 types of dendrite geometries ("dendritic

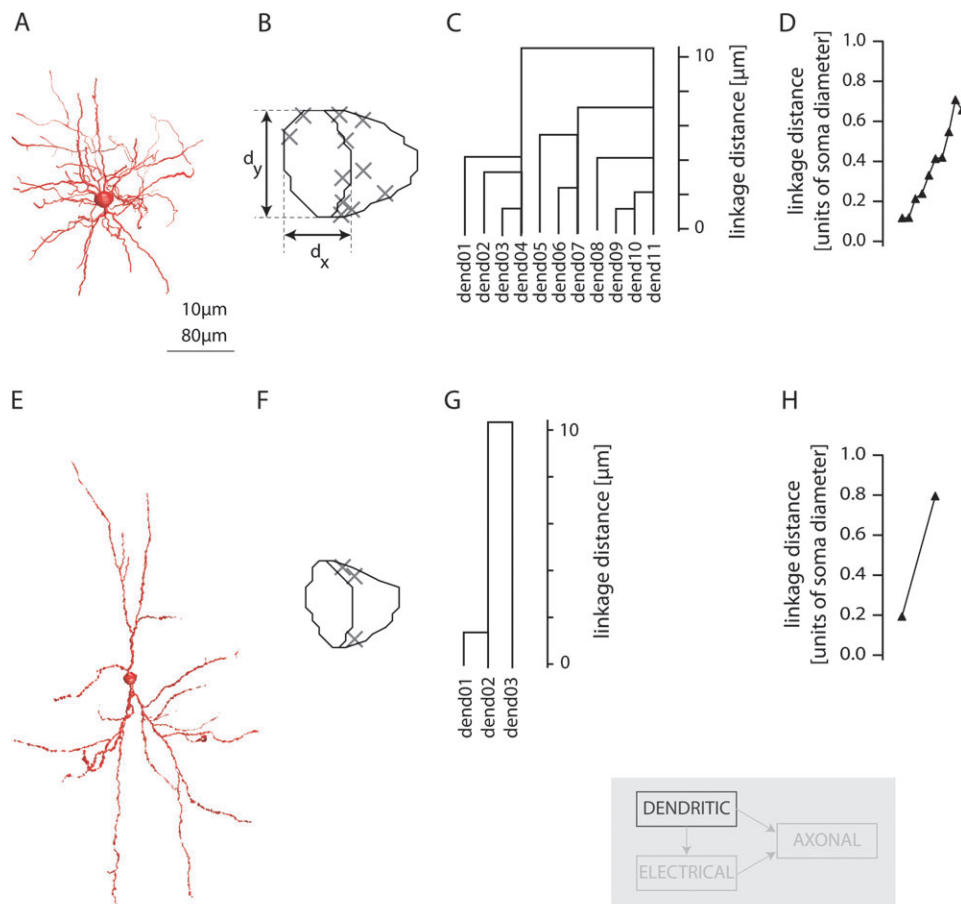


Figure 1. Quantification of dendritic polarity. (A, E) Three-dimensional cylindrical approximation of dendritic geometries of 2 L2/3 interneurons. (B, F) Map of the surface of the somata (black outline) with insertion points of primary dendrites indicated by crosses. The surface map is a cylinder projection of the soma surface with the cylinder oriented along the y -axis perpendicular to the brain surface. The axis conventions are indicated in (B): d_x points along the horizontal axis, d_y along the vertical axis. Longitudinal meridians are parallel to d_y ; horizontal meridians are parallel to d_x . (C, G) Linkage plots of CAs that were made on the x , y , and z -coordinates of the insertion points of primary dendrites on the somatic surface. (D, H) The largest linkage distance was normalized to the larger soma diameter $\max(d_y, d_x)$. All subsequent linkage distances were normalized to the smaller soma diameter $\min(d_y, d_x)$. The distribution of linkage distances normalized in this way was used to compute a one-dimensional measure of dendritic polarity “dendritic polarity index” (for details, cf. Results and Methods).

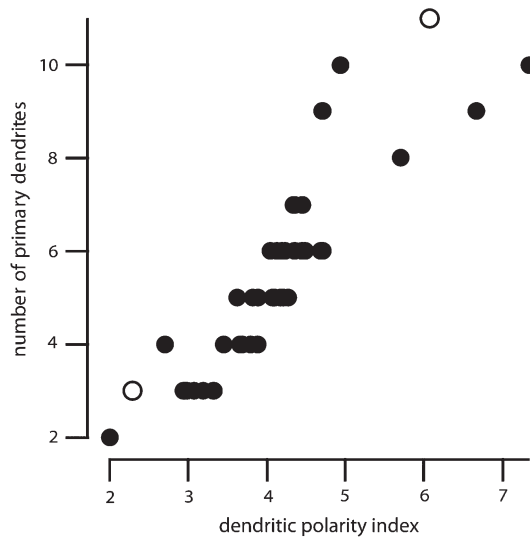


Figure 2. Correlation between the number of primary dendrites and the dendritic polarity index ($r = 0.91$, $P < 10^{-6}$). Open circles indicate the 2 neurons shown in Figure 1.

types” shown in Supplementary Figs 3–6). We then evaluated the relation between this high-dimensional measure of dendrite geometry and the one-dimensional dendrite polarity index derived above. Figure 4B shows the dendritic polarity index for the 7 dendritic types, which was significantly different between types (ANOVA, $P < 0.0005$; a post hoc Newman–Keuls test showed that clusters 1,2 were significantly different from clusters 6,7, $P < 0.05$).

Dendritic Polarity and Electrical Membrane Properties

Subsequently, we investigated the relation between dendritic polarity and electrical membrane properties using measures of intrinsic electrical excitability that have been employed in many studies (e.g., Connors and Gutnick 1990). Figure 5A shows the AP discharge patterns of 2 inhibitory neurons in response to 500-ms depolarizing current pulses. The dendritic reconstructions and soma surface plots of the 2 cells are shown in Figure 5B. We analyzed 5 relevant characteristics of AP discharge patterns: 1) The AP frequency adaptation ratio at about 100-Hz initial spike frequency (Fig. 5C), 2) adaptation of the AP-AHP in the same 100-Hz trace (Fig. 5D), 3) AP half

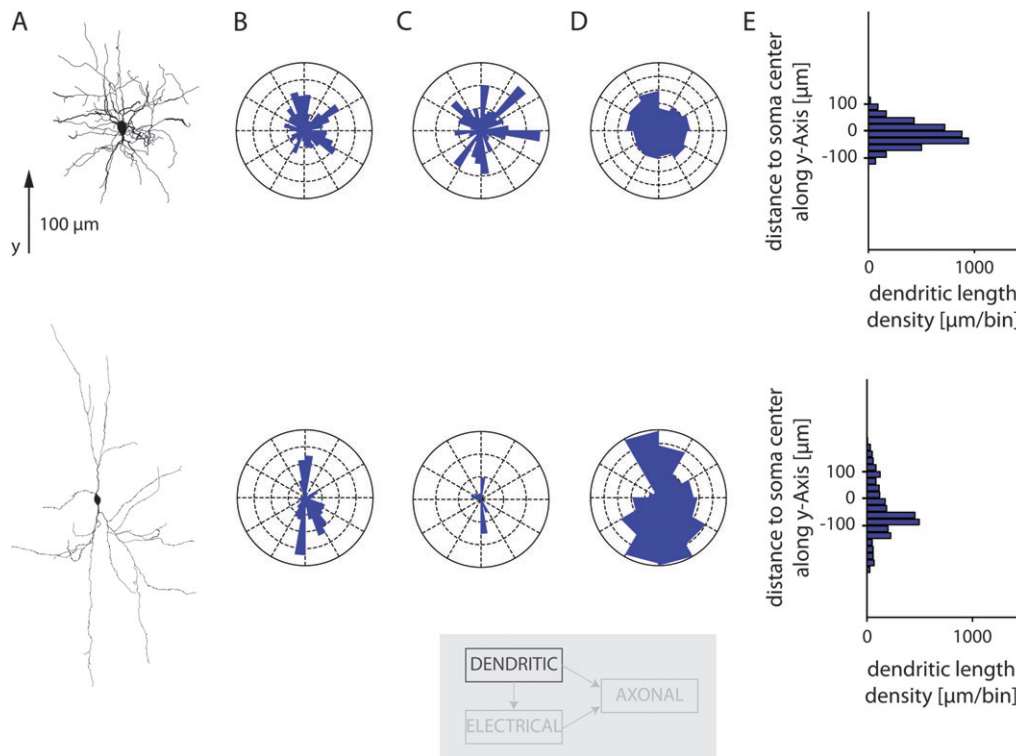


Figure 3. Detailed quantification of dendritic geometry. Two example neurons are shown in (A) as 2D-projected reconstructions (same neurons as in Fig. 1). (B) Angular distribution of dendritic path length for the 2 neurons shown in (A), centered at the soma center. Bin size 10° , the 3D dendritic path lengths were integrated along the z-axis. One radial tick corresponds to a path length of $100 \mu\text{m}/10^\circ$ bin (total of 36 bins). (C) Angular distribution of dendritic length within a sphere of $30 \mu\text{m}$ radius from the soma center. One radial tick corresponds to a path length of $20 \mu\text{m}/10^\circ$ bin, same bin conventions as in (B) (total of 36 bins), (D) maximum extent of the dendritic field, measured in the plane of the slice with bin size 30° . One radial tick corresponds to $50\text{-}\mu\text{m}$ Euclidean distance from the soma center (total of 12 bins). (E) Dendritic path length density along an axis perpendicular to the pial surface (bin size $25 \mu\text{m}$, total of 17 bins).

widths (Fig. 5E), 4) AP threshold, and 5) the apparent somatic input resistance measured as I/V ratio for assumedly passive membrane potentials around V_{rest} (not illustrated; for details of the analysis, cf. Methods).

We found a strong correlation between dendritic polarity and AP frequency adaptation ratio (Fig. 6A, $r = 0.49$, $P < 0.005$). Interneurons with positive AP frequency adaptation ratios (i.e., an increase in AP frequency during the train) had a high dendritic polarity index (≥ 4). The number of primary dendrites was also highly correlated with AP frequency adaptation ratio ($r = 0.55$, $P < 0.0001$, Fig. 6B).

This correlation between the number of primary dendrites and AP frequency adaptation ratio could be either purely correlative, or could represent a direct causal effect of the morphology on electrical properties. We therefore investigated by numerical simulations, to what degree the dendritic morphology alone can account for these correlations.

The interneuron shown in the left panels of Figure 7A,B had 7 primary dendrites (polarity index 4.3) and had a positively adapting AP pattern (AP frequency adaptation ratio = +0.7). The interneuron shown in the right panels of Figure 7A,B had 4 primary dendrites (polarity index = 2.7) and a negatively adapting firing pattern (AP frequency adaptation ratio = -1). The dendritic arbors were used in a multicompartment numerical model with a normalized set of conductance distributions (Mainen and Sejnowski 1996; Schaefer et al. 2003) assuming Na^+ , K^+ , K^+_{Ca} , Ca^{2+} -conductances with

constant densities for the soma, dendrites and a prototypic axon, respectively. The absolute values of conductance densities were adjusted such that 4 control pyramidal neurons showed a strongly adapting firing pattern (not shown). Figure 7C shows the AP firing patterns that were simulated for the 2 interneurons shown in Figure 7A,B with this set of conductances (conductance set 1). All electrical parameters were similar between the 2 neuron simulations, except for the geometry of the soma and dendrites as shown in Figure 7B. The examples indicate that the dendritic geometry can partially account for differences in AP frequency adaptation ratios.

Then, these numerical simulations were made in all interneurons, and AP frequency adaptation ratio was measured in each of these simulations. Figure 8A shows the relation between the simulated AP frequency adaptation ratio and the number of primary dendrites, which were significantly correlated ($r = 0.38$, $r^2 = 0.14$, $P < 0.01$, $n = 53$). When compared with the experimentally measured correlation between AP frequency adaptation ratio and the number of primary dendrites (Fig. 6B, $r^2 = 0.3$), the simulations could thus account for up to 50% of the experimentally measured correlation between AP frequency adaptation and the number of primary dendrites. Figure 8B shows the relation between the simulated and the measured AP frequency adaptation ratios. Results for pyramidal neurons are indicated by open triangles for comparison. Results for different sets of conductances are shown in the Supplemental Material.

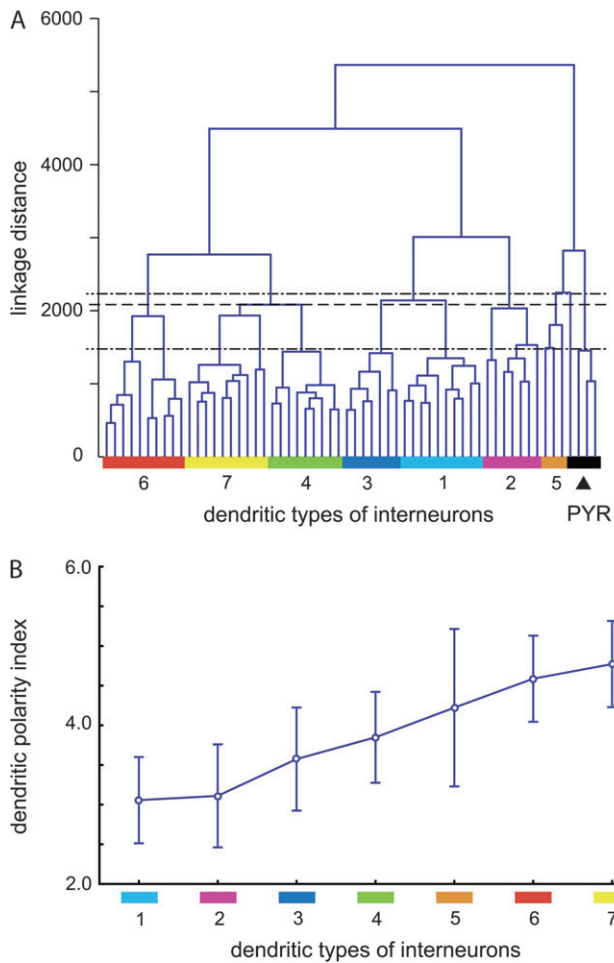


Figure 4. Clustering of dendritic types in the 101-parameter space illustrated in Figure 3. (A) Linkage plot of the CA (Ward's method, Euclidean distances). Four pyramidal neurons were included as control group. Cluster cutoff (dashed line) was determined such that pyramidal neurons were linked together (upper limit; upper dot-dashed line) and were not linked to interneurons (lower limit; lower dot-dashed line). Variation of the cutoff within these limits did not alter the correlation results shown below. For details cf. Results and Methods. (B) Correlation of dendrite types as determined in A with the one-dimensional polarity index (Figs 1, 2). The 7 types of dendritic geometries had different dendritic polarity indices (ANOVA, $P < 0.0005$; error bars indicate 95% confidence limits; in a post hoc Newman-Keuls test, dendritic types 1 and 2 were significantly different from types 6 and 7; $P < 0.05$).

Dendritic Geometry and Axonal Projection Types

Next, the relation between dendritic polarity and the axonal projection geometry was investigated. Figure 9A,B shows the axonal projection of the 2 interneurons illustrated in Figure 1. The neuron with a high dendritic polarity index ($=6.1$) had a local axonal projection in layer 2/3 (Fig. 9A), whereas the neuron with a bipolar dendritic polarity index ($=2.3$) projected vertically within the home column (Fig. 9B). Figure 9C shows the relation between dendritic polarity and *verticality* of axonal projection (*verticality* was quantified as the ratio of axonal path length extending below layer 2/3 within the home column, cf. Helmstaedter et al. 2008a). Dendritic polarity was only weakly correlated with *verticality* of axonal projection ($r = -0.37$, $P < 0.02$, Figure 9C, the correlation was outlier-dominated, rank correlation was not significant). Dendritic polarity was also not correlated with *laterality* of axonal projection ($r = 0.07$, Fig. 9D; *laterality* was quantified as the

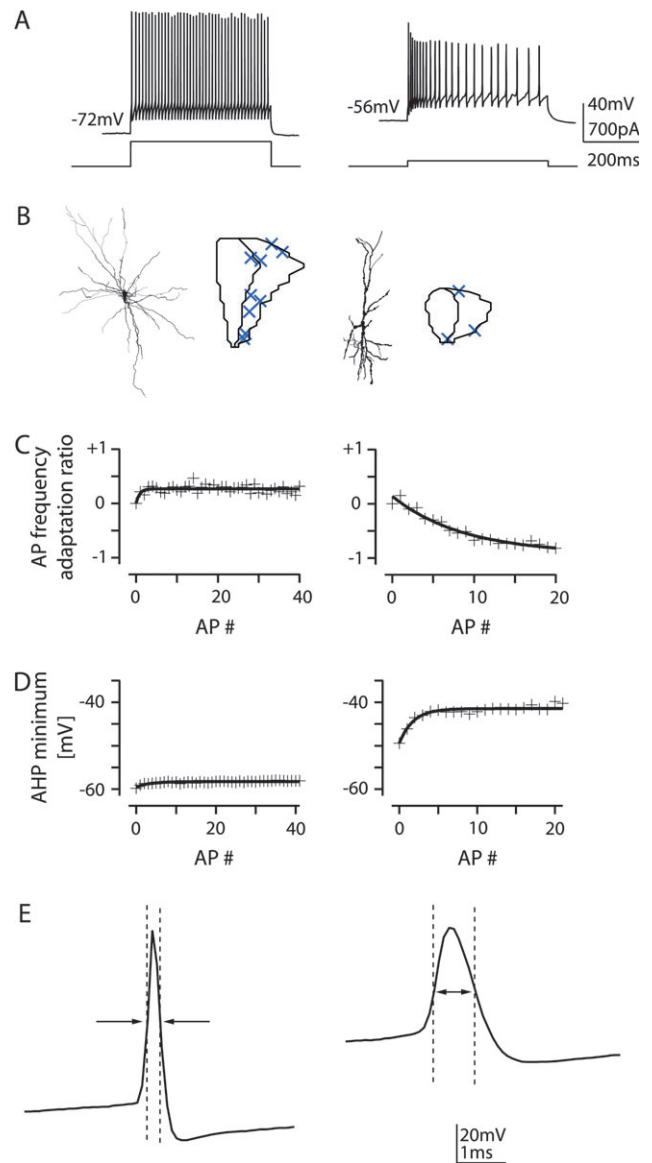


Figure 5. Quantification of intrinsic electrical excitability. (A) Trains of APs evoked by somatic current injection in 2 interneurons (dendritic geometries shown in B). The trace with a first interspike interval (ISI) of approximately 10 ms was chosen for analysis ("100-Hz trace"). (C) Analysis of AP frequency adaptation ratio in the 2 trains of APs shown in A. ISIs were converted to AP frequencies and normalized to the first frequency (crosses). The relative change is shown. AP frequencies were fitted to a monoexponential function, and the ratio of the last fitted point to the first fitted point minus 1 was interpreted as AP frequency adaptation ratio. (D) Analysis of AHP amplitude evolution. The minimum voltage between APs was recorded over the train of APs. A monoexponential function was fitted to the data, and the difference between the last fitted point and the first fitted point was recorded as AHP adaptation. (E) AP half width was measured as the width of the AP at half-maximal amplitude, and averaged for all APs in the 100-Hz train of APs (shown in A).

ratio of axonal path length extending to neighboring columns, cf. Helmstaedter et al. 2008a).

The weak parametric correlation between dendritic polarity and axonal *verticality* was mainly caused by 3 cells with vertical axon projections and a low polarity index <3 and a group of 4 cells with no vertical axon projection and a high polarity index >5 (without these cells: $r = 0.04$). It is important to note that for the majority of interneurons this correlation did not allow to predict axonal projection patterns. "Bipolar" or

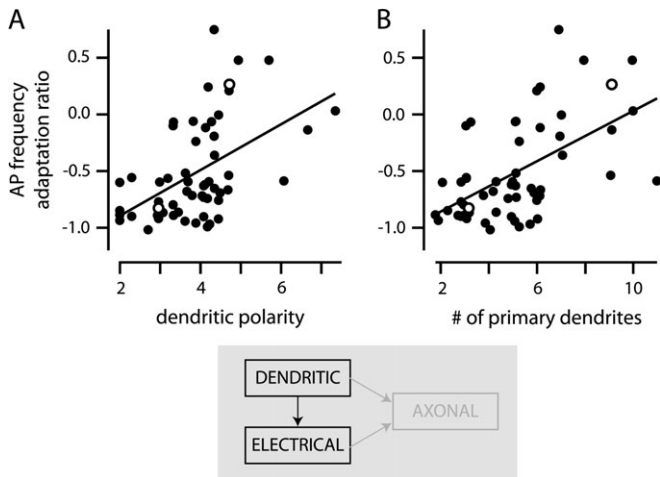


Figure 6. Relation of dendritic geometry and electrical excitability. (A, B) The ratio of AP frequency adaptation was correlated with dendritic polarity ($r = 0.49$, $P < 0.005$, (A) and to the number of primary dendrites ($r = 0.55$, $P < 0.0001$, (B)). Open circles indicate data from the 2 neurons shown in Figure 7.

“tripolar” cells could both be highly vertical or entirely locally projecting (Fig. 9C). Dendritic polarity was thus not a predictor of *verticality* or *laterality* of axonal projection.

To validate this finding we also investigated whether the 7 dendritic types were related to the 3 main axonal projection types found in the previous study (Helmstaedter et al. 2008a). Figure 10A shows the axonal laterality and verticality of the 7 dendrite geometry types as determined above (color code in Fig. 10A). There was no significant difference in axonal laterality and verticality among the 7 dendritic types (ANOVA, $P > 0.05$). Figure 10B shows the complementary distribution of the axonal types in the dendritic parameter space (reduced to its first 3 principal components for display). As a fourth test we measured the canonical correlation between 4 dendritic parameters (number of primary dendrites, total dendritic length, dendritic polarity index, length per primary dendrite, cf. Table 1) and the 2 axonal parameters (laterality and verticality). No multidimensional correlation could be detected (Fig. 10C, $P > 0.07$, cf. Methods). We conclude that dendritic density is not a predictor of axonal projection types.

Clustering of Electrical Membrane Properties

We next investigated whether electrical membrane properties that were measured in many previous studies allowed a definition of interneuron classes in the unselected sample of L2/3 interneurons. Interneurons with positive AP frequency adaptation and small AP half width have been previously defined as “fast-spiking (FS)” cells (e.g., Kawaguchi 1993; Kawaguchi and Kubota 1993). Figure 11A shows the correlation between AP half width and AP frequency adaptation ($r = -0.37$, $P < 0.005$). Positive frequency adaptation ratios predict half widths of < 0.6 ms. A CA suggested 2 clusters (e.g., FS vs. non-FS cells, cf. inset in Fig. 11A). Figure 11B shows the correlation between somatic input resistance and AP half width ($r = 0.46$, $P < 0.0005$) that was also suggested to define FS cells (Kawaguchi 1993; Kawaguchi and Kubota 1993). This distribution was, however, only weakly clustered.

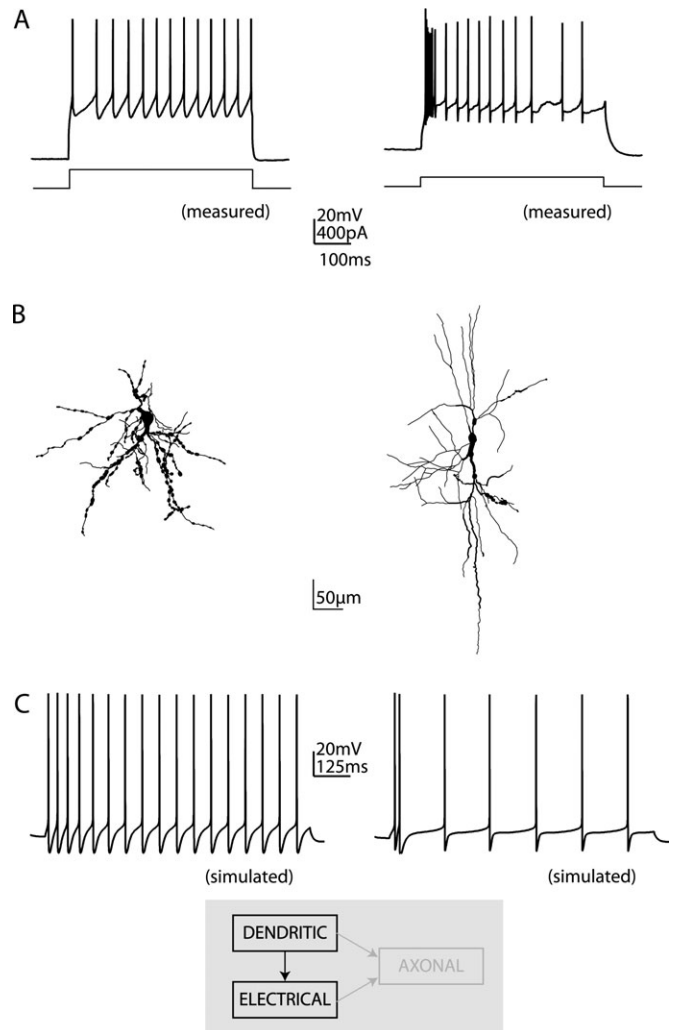


Figure 7. Numerical simulations of firing patterns. (A) Two traces of APs recorded in the neurons shown as dendritic reconstructions in (B). (C) Numerical simulations (using NEURON) in the 2 neurons with the same set of voltage-gated conductances at the same density showed 2 distinct firing patterns. The conductance set was calibrated in a group of control pyramidal neurons. For simulations using a second set of conductance densities that was calibrated by the average input resistance of interneurons, cf. Supplemental Material. For details see Results.

Electrical Membrane Properties and Axonal Projection Types

We then examined whether electrical membrane properties could be matched to axonal projection types (defined by the projection of L2/3 interneuron axons with reference to cortical columns; Helmstaedter et al. 2008a). Briefly, the axons of L2/3 local inhibitors projected to L2/3 of the home column; L2/3 lateral inhibitors projected to a significant degree to L2/3 of the surround columns; the axons of L2/3 translaminar inhibitors projected to a significant degree to L4 and L5 of the home column. Figure 11A,B shows the distribution of local, lateral, and translaminar inhibitors in the relation between AP half width, AP frequency adaptation ratio and input resistance. Figure 11C shows the distribution of local, lateral, and translaminar inhibitors in the space of electrical excitability parameters (depicted in their first 3 principal components, cf. Table 2). Local, lateral and translaminar

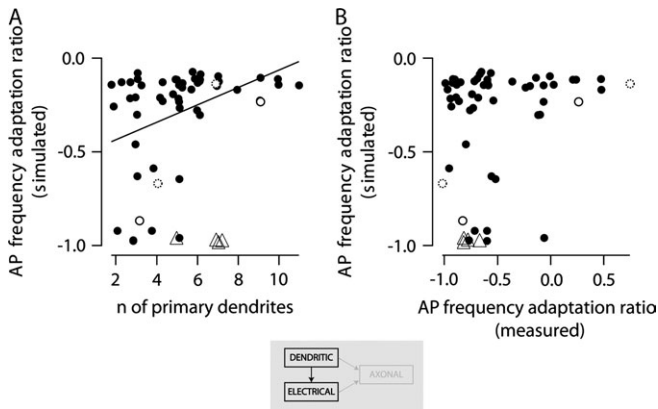


Figure 8. Dendritic morphology could explain variability in AP firing. (A) Correlation between AP frequency adaptation ratio in trains of APs that were obtained in numerical simulations in the dendritic geometries of 51 interneurons and the number of primary dendrites ($r = 0.38$, $P < 0.01$). Conductance distributions were equal for all cells (conductance set as in Fig. 7), thus differences in somatic and dendritic geometry were the only source of variability in these simulations. Data from 4 control pyramidal neurons is shown as triangles. (B) Comparison between simulated and measured AP frequency adaptation ratio.

inhibitors showed no significant differences in electrical excitability parameters (ANOVA, $P > 0.29$, Fig. 11A-C Supplementary Fig. 7, color code). Figure 11D shows the canonical correlation between the 5 major electrical excitability parameters (see above) and axonal projection patterns. As there was no significant correlation ($P > 0.1$, cf. Methods), we conclude that the suggested classifications of interneurons by electrical excitability parameters could not predict the type of axonal projections.

Electrical Membrane Properties, Dendritic Geometry, and Axonal Projections

We finally tested whether the combination of electrical and dendritic parameters could predict the type of axonal projection. Figure 12A shows the distribution of *local*, *lateral* and *translaminar inhibitors* in the first 3 principal components of the combined dendritic and electrical excitability parameter space. The canonical correlation analysis (Fig. 12B) still showed no predictive capacity ($r^2 < 0.25$, $P > 0.1$, cf. Methods).

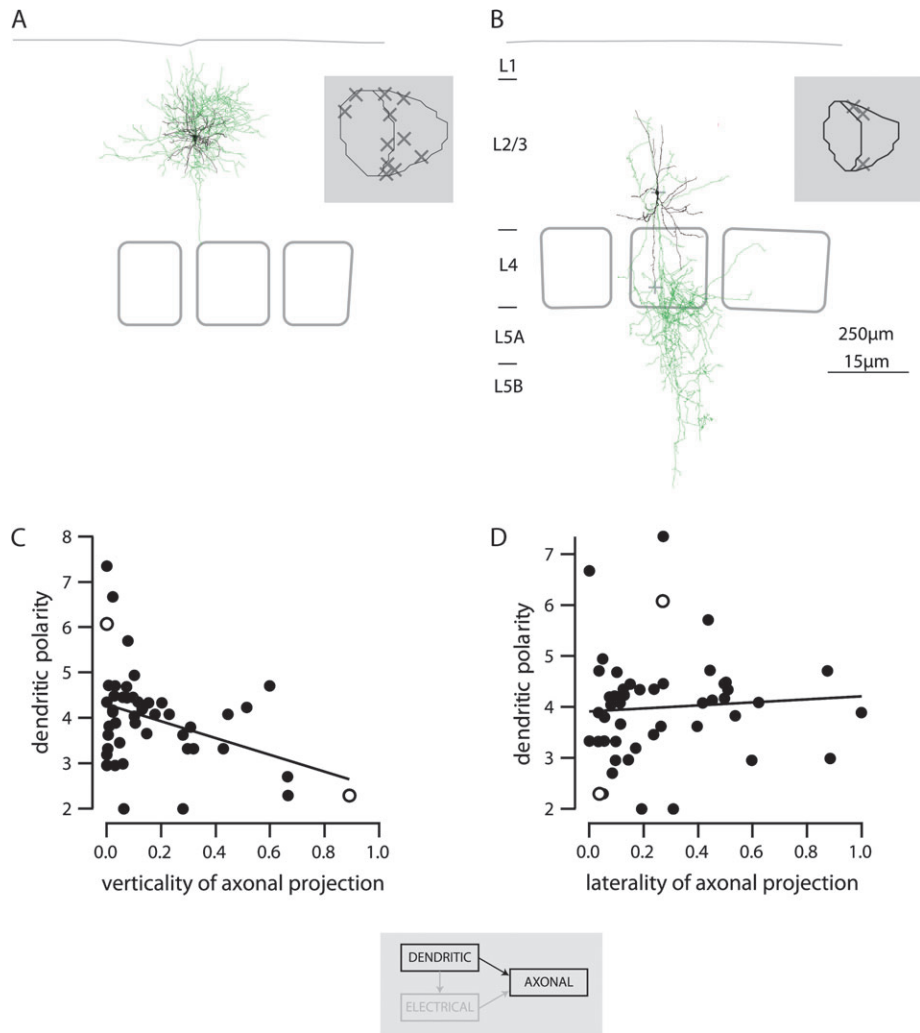


Figure 9. Relation of axonal projection to dendritic polarity. (A, B) reconstructions of axonal and dendritic arbors of the 2 L2/3 interneurons shown in Figures 1 and 3. The 2 examples suggested a relation between high polarity index and local axonal projection (A) versus low polarity index and vertical axonal projection (B). (C) Dendritic polarity and axonal verticality were weakly correlated in the complete population ($r = -0.37$, $P < 0.02$, open circles, neurons in A, B). For details see Results. (D) Dendritic polarity was not correlated to the laterality of axonal projection ($r = 0.07$).

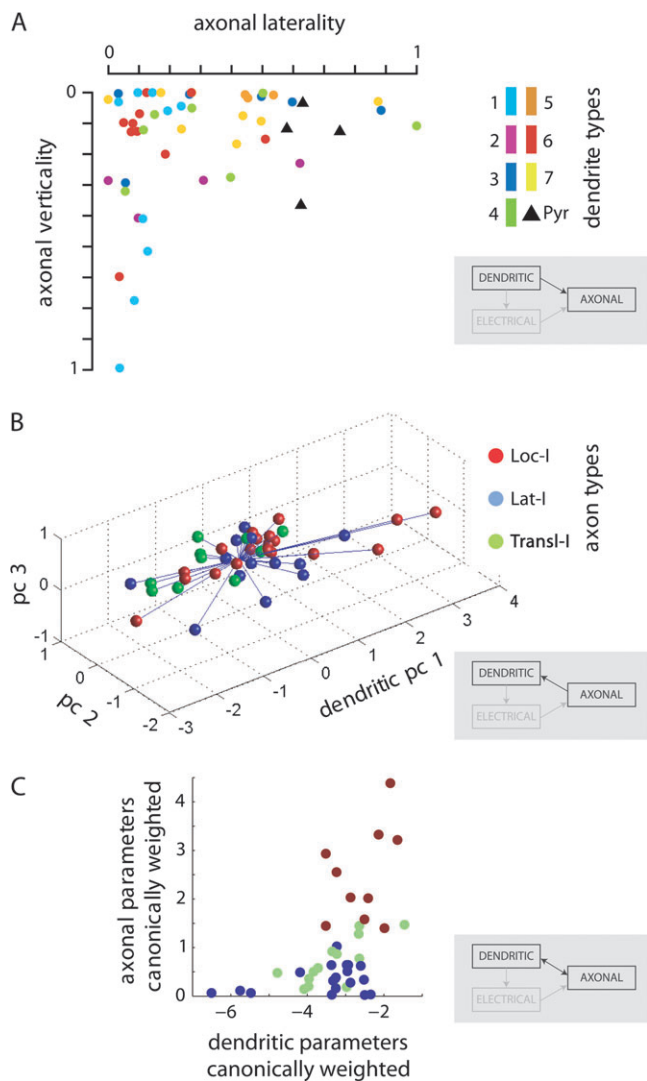


Figure 10. Multidimensional relations of dendritic geometry and axonal projection types. (A) Distribution of types of dendritic geometries (cf. Fig. 4, color code) in the 2D space of axonal laterality and verticality. Dendritic types were not different in these axonal properties (ANOVA, $P > 0.05$). (B) Distribution of types of axonal projection (Helmstaedter et al., 2008a; cf. Table 1) in the 3D space of the first 3 principal components of the 4 dendritic parameters (number of primary dendrites, total dendritic length, dendritic polarity index, length per primary dendrite). (C) Canonical correlation of axonal parameters (laterality, verticality) and dendritic parameters (as in B). There was no multidimensional correlation ($P > 0.07$). Importantly, dendritic parameters were not predictive of axonal parameters.

Discussion

Experimental Constraints

The measurement of multiple morphological, electrical excitability, and antigen expression parameters in neocortical interneurons represents a major challenge: the concurrent measurement of many of these parameters is hardly feasible, neither in vitro nor in vivo. Therefore, in many studies only a subset of the available parameters (often pairs of parameters) could be used for the definition of neuron identity. Findings were related to the classification in this highly reduced parameter space (Beierlein et al. 2000, 2003; Cauli et al. 2000; Porter et al. 2001; Wang et al. 2002; Bacci et al. 2004;

Table 1
Summary of dendritic parameters

Types	Dendritic polarity (a.u.)	n of primary dendrites	Length per primary dendrite (μm)	Total dendritic length (mm)
Local inhibitors ($n = 19$)	$4.4 \pm 28\%$	$6.1 \pm 41\%$	$550 \pm 52\%$	$2.8 \pm 21\%$
Lateral inhibitors ($n = 14$)	$4 \pm 21\%$	$5.7 \pm 35\%$	$670 \pm 50\%$	$3.5 \pm 38\%$
Translaminar inhibitors ($n = 10$)	$3.4 \pm 23\%$	$4 \pm 31\%$	$700 \pm 29\%$	$2.7 \pm 26\%$
L1 inhibitors ($n = 4$)	$3.6 \pm 18\%$	$4.2 \pm 35\%$	$860 \pm 52\%$	$3.2 \pm 29\%$
All ($n = 57$)	$3.9 \pm 27\%$	$5.1 \pm 42\%$	$660 \pm 48\%$	$2.9 \pm 33\%$

Note: Data are reported as mean \pm SD pooled by the types of axonal projection (cf. Helmstaedter et al. 2008a). Briefly, L2/3 local inhibitors projected to L2/3 of the home column; L2/3 lateral inhibitors projected a significant part of the axon to L2/3 of the surround columns; L2/3 translaminar inhibitors projected a significant part of their axon to L4 and L5 of the home column. SD is reported in percent of mean to allow comparison of parameter homogeneity between types. For statistical analysis cf. Results and Figures 10–12.

Toledo-Rodriguez et al. 2005; Dumitriu et al. 2007). The present study was aimed at an unbiased quantitative analysis of the low-dimensional relations between interneuron properties (i.e., between pairs, triplets or quadruplets of parameters). The goal was to find out whether small (2–5) sets of parameters could be used as valid predictors of higher-dimensional classifications. We found that dendritic geometry was partly predictive of intrinsic electrical excitability, as expected from previous simulation studies comparing electrical excitability in excitatory and inhibitory neurons with strongly differing morphologies (Mainen and Sejnowski 1996). Our results suggest, however, that axonal projection patterns are almost independent of dendritic geometry or electrical excitability parameters. These findings are consistent with a series of studies that used quantitative methods for the analysis of electrophysiological or dendritic classes of neurons (Nowak et al. 2003; Krimer et al. 2005; Zaitsev et al. 2005). A quantitative definition of electrophysiological types did only partially correlate with immunohistochemical marker expression. It did not allow a prediction of qualitative morphological properties in monkey dorsolateral prefrontal cortex (Zaitsev et al. 2005). In a second study from the same preparation, electrophysiologically defined classes of interneurons did not predict the qualitative description of axonal and dendritic geometry (with the exception of chandelier neurons, Krimer et al. 2005). This was also found in in vivo recordings from cat visual cortex (Nowak et al. 2003).

Limitations of the In Vitro Slice Preparation

The morphological analysis of neurons stained intracellularly in vivo provides reconstructions of complete axonal arbors with isotropic distribution, including longer-range projections spanning several millimeters (e.g., Bruno and Sakmann 2006). Although in vivo staining of excitatory neurons is well feasible, there are only very few reports of reconstructions of interneurons stained in vivo (e.g., Hirsch et al. 2003). Therefore, a quantitative analysis of interneuron morphology on a sufficiently large sample ($n > 30$) had to be done in an in vitro preparation. Errors introduced by the in vitro slice preparation include 1) putative truncation of axons or dendrites; 2) anisotropic shrinkage during fixation (especially in the direction normal to the coverslip, cf. Egger et al. 2008); 3) introduction of a direction bias by the choice of the slice plane. We attempted to minimize these artifacts by 1) quantitative

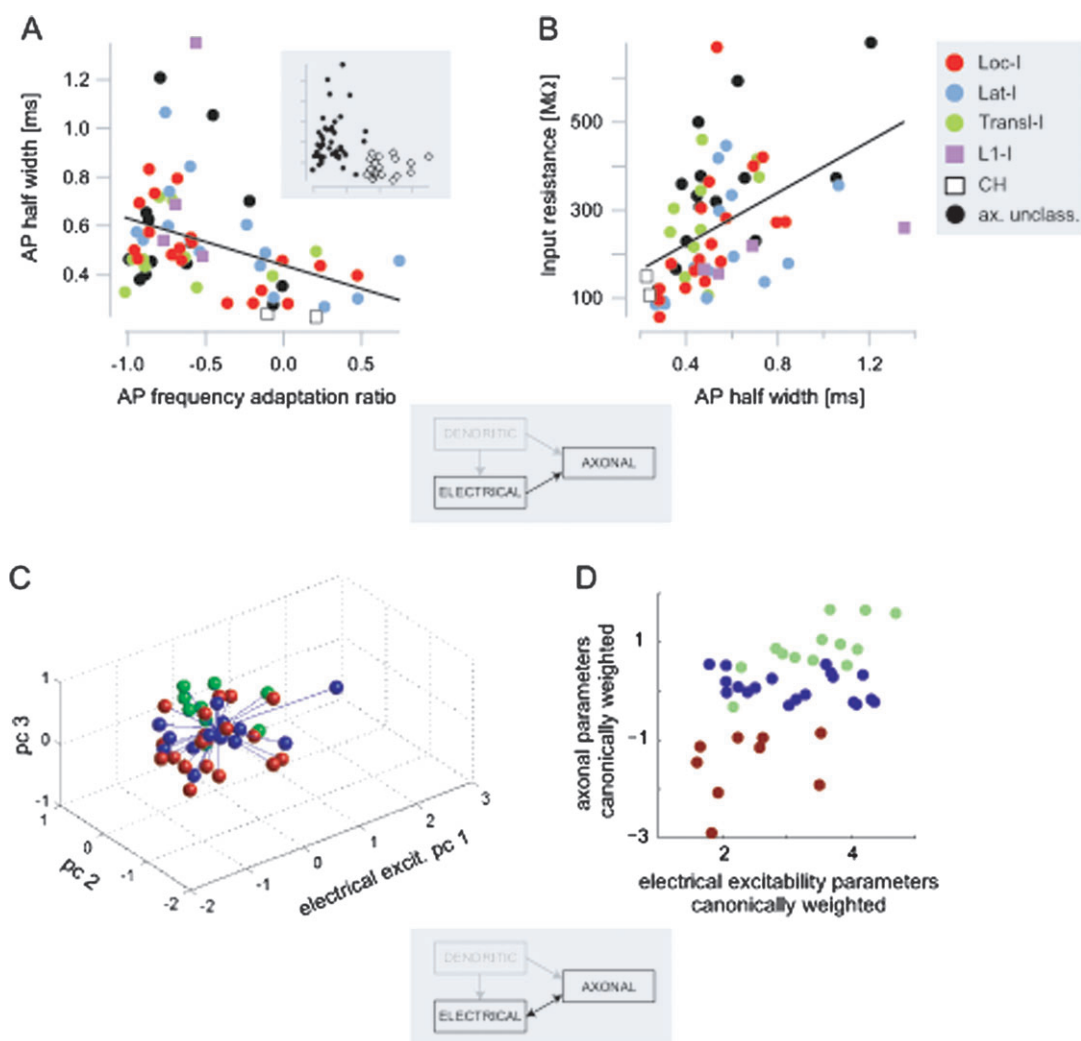


Figure 11. Multidimensional relations between electrical excitability parameters and axonal projections. (A) Relation of AP half width and AP frequency adaptation ratio. The relation allowed to define 2 clusters by CA (cf. inset). The color code indicates the axonal projection type of the neurons. The 3 types of axonal projection (local, lateral, and translaminal inhibitors, cf. Helmstaedter et al., 2008a) were not different with respect to AP half width and AP frequency adaptation ratio. (B) Correlation of apparent input resistance at the soma and AP half width ($r = 0.46$, $P < 0.0005$). (C) Relation between all 5 electrical parameters and the axonal projection types (color code as in A). The electrical parameters are displayed in their first 3 principal components. There was no statistical difference of axonal projection types with respect to the 5 electrical parameters used (color code, ANOVA, $P > 0.3$). (D) Canonical correlation analysis of the relation between the set of electrical excitability parameters and the axonal parameters. The relation was not significant ($P > 0.1$) and not predictive ($r^2 < 0.12$).

Table 2

Summary of electrical parameters

		Input resistance (GΩ)	AP half width (ms)	AP frequency adaptation ratio	AHP adaptation (mV)	AP threshold potential (mV)
Types						
Local inhibitors	($n = 19$)	$0.24 \pm 59\%$	$0.51 \pm 32\%$	$-0.48 \pm 89\%$	$0.98 \pm 350\%$	$-44 \pm 16\%$
Lateral inhibitors	($n = 15$)	$0.22 \pm 56\%$	$0.55 \pm 38\%$	$-0.33 \pm 158\%$	$2.4 \pm 149\%$	$-45 \pm 16\%$, $n = 13$
Translaminal inhibitors	($n = 10$)	$0.29 \pm 39\%$	$0.48 \pm 27\%$	$-0.63 \pm 63\%$	$1.6 \pm 180\%$	$-52 \pm 7\%$, $n = 9$
L1 inhibitors	($n = 4$)	$0.2 \pm 24\%$	$0.76 \pm 52\%$	$-0.64 \pm 18\%$	$7.9 \pm 46\%$	$-46 \pm 21\%$, $n = 2$
All	($n = 64$)	$0.26 \pm 53\%$	$0.54 \pm 41\%$	$-0.5 \pm 86\%$	$2.1 \pm 171\%$	$-46 \pm 17\%$, $n = 56$

Note: Data are reported as mean \pm SD pooled by the types of axonal projection (cf. Helmstaedter et al., titled "Neuronal correlates of lateral, local and translaminal inhibition with reference to cortical columns"). Standard deviation is reported in percent of mean to allow comparison of parameter homogeneity between types. For statistical analysis cf. Results and Figures 10, 11.

criteria for inclusion of reconstruction based on the total axonal path length (cf. Methods); 2) usage of very thin glass coverslips, and projection of the measured 3D path lengths into the plane of the slice for analysis; 3) choice of a slice plane and slice thickness that presumably contains one cortical column

(z -direction) and at least 2 neighboring cortical columns (x -direction). In addition, the term dendritic polarity is usually employed for polarity along an axis perpendicular to the cortical surface (e.g., Jones 1975). Thus, for the measures analyzed in this study, the projection of dendritic path length

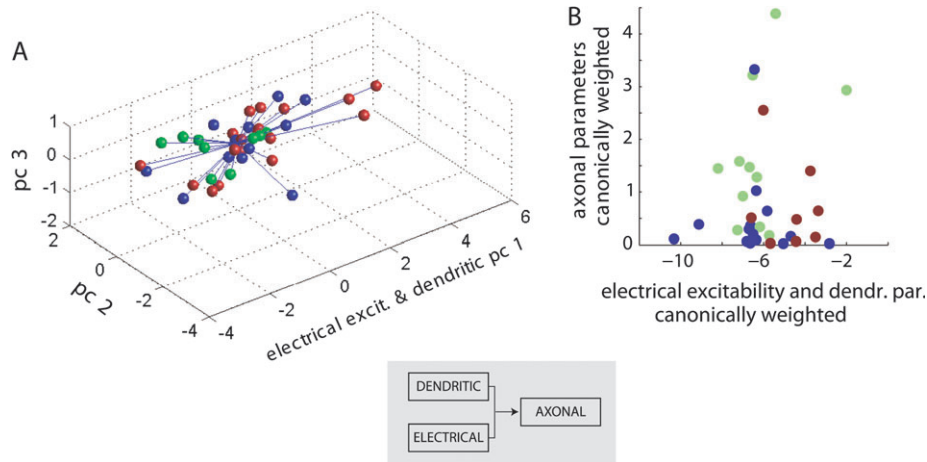


Figure 12. (A) Electrical excitability and dendritic geometry parameters were combined to test for prediction of *axonal projection types*. The 9-parameter space is shown in its first 3 principal components. *Axonal projection types* are color-coded (see Fig. 11). (B) The canonical correlation of the combined set of electrical and dendritic parameters was weak and not predictive ($r^2 < 0.25$).

into the plane of the slice could be expected to introduce only minor artifacts (for details, cf. Methods).

Comparison to Previous Studies of Dendritic Geometry

We have presented approaches for quantifying dendritic geometry. A multidimensional approach included the radial and vertical distribution of dendritic densities around the soma. In qualitative descriptions of dendritic shape, typically, “bipolar” geometries were distinguished from “bitufted” geometries (Kawaguchi and Kubota 1997; Feldman and Peters 1978; Porter et al. 1998). Although both types were described as having bipolar dendritic origins, bitufted geometries were defined to show extensive branching at a particular distance from the soma. All of these features should be captured in the set of radial and vertical dendritic density distributions (cf. Fig. 3). However, the unsupervised clustering did not yield 2 distinct populations of bipolar versus bitufted dendritic geometries in our sample (cf. Supplementary Material Figs 3–6, types 1,2,4 for illustration). It may be speculated that the distinction of bitufted versus bipolar dendritic geometries is not a valid classifier of interneurons. Our quantitative classification of dendritic types also yielded types with similarities to large multipolar basket cell dendrites (types 5,7; Supplementary Figs 5 and 6; Fairén et al. 1984), to neurogliaform neurons (dendritic type 6, Supplementary Fig. 5; Jones 1984), and to tripolar neurons with a major descending dendrite (dendritic type 3, Supplementary Fig. 4).

Correlation between Dendritic Geometry and Electrical Excitability

The electrical excitability of a neuron can be properly modeled by cable theory using the geometry of the soma, dendrites and axon, as well as the distribution of transmembrane conductances along the neuron’s membrane (e.g., Rall 1959; Koch 1999). Both the geometry and the conductance distributions are thus causal for the electrical excitability measured at the soma. This causality was first quantified for the variability between cell types by Mainen and Sejnowski (1996). Schaefer et al. (2003) showed that specific morphological parameters (the number

and position of oblique dendrites) could be predictive of specific functional properties of pyramidal cells (i.e., the likelihood of calcium-spikes in the distal apical dendrites). Here, we showed that the morphological variability within a cell class, L2/3 interneurons, could explain a large fraction of the variability in electrical excitability (i.e., in the AP discharge patterns measured at the soma). Therefore, electrical excitability and dendritic geometry cannot be considered as independent classifiers of interneurons. Instead we show that axonal projection types were such independent classifiers.

Comparison to Classifications of Hippocampal Interneurons

The attempts of classification of hippocampal interneurons have been more successful in finding clear correlations between dendritic geometry and axonal projections (for a review, see e.g., Somogyi and Klausberger 2005). This may be due to a more clearly defined stratification into layers in the hippocampus. Layers in the hippocampus correspond to defined parts of pyramidal neurons in CA1 (soma, basal dendrites, apical dendrites). Axonal projections of hippocampal interneurons have been shown to be restricted to single layers of the hippocampus, resulting in subcellular specificity of axonal projections (for reviews: McBain and Fisahn 2001; Whittington and Traub 2003; Jonas et al. 2004). In contrast, the spatial precision of intracortical axonal projections is not yet fully understood (e.g., Di Cristo et al. 2004; Douglas and Martin 2007).

Surrogate Parameters

Low-dimensional subsets of parameters can only be used as surrogates for higher-dimensional classifications if they have been shown to be predictors of this higher-dimensional classification in an unselected sample of neurons. Typically employed surrogate parameter sets (Beierlein et al. 2000, 2003; Cauli et al. 2000) could not be shown to be sufficient for this requirement in our data set. Thus, low-dimensional classifications for neocortical interneurons have to be questioned and a multidimensional analysis is needed to define interneuron

groups (cf. the accompanying study; Helmstaedter et al. 2008b).

Supplementary Material

Supplementary material can be found at: <http://www.cercor.oxfordjournals.org/>

Funding

This work was supported by the Max-Planck Society.

Notes

We would like to thank Drs Jochen Staiger, Arnd Roth, Andreas Schaefer and Idan Segev for fruitful discussions, and Drs Jochen Staiger and Andreas Schaefer for helpful comments on previous versions of the manuscript, Ms Marlies Kaiser for expert technical assistance and Jonas Tesarz for help with reconstructions. *Conflict of Interest:* None declared.

Address correspondence to Moritz Helmstaedter, Department of Cell Physiology, Max-Planck Institute for Medical Research, Jahnstr. 29, D-69120 Heidelberg, Germany. Email: moritz.helmstaedter@mpimf-heidelberg.mpg.de.

References

- Agmon A, Connors BW. 1991. Thalamocortical responses of mouse somatosensory (barrel) cortex in vitro. *Neuroscience*. 41:365–379.
- Ascoli GA, Alonso-Nanclares L, Anderson SA, Barrionuevo G, Benavides-Piccione R, Burkhalter A, Buzsaki G, Cauli B, DeFelipe J, Fairen A, et al. 2008. Petilla terminology: nomenclature of features of GABAergic interneurons of the cerebral cortex. *Nat Rev Neurosci*. 9:557–568.
- Bacci A, Huguenard JR, Prince DA. 2004. Long-lasting self-inhibition of neocortical interneurons mediated by endocannabinoids. *Nature*. 431:312–316.
- Beaulieu C. 1993. Numerical data on neocortical neurons in adult rat, with special reference to the GABA population. *Brain Res*. 609:284–292.
- Beierlein M, Gibson JR, Connors BW. 2000. A network of electrically coupled interneurons drives synchronized inhibition in neocortex. *Nat Neurosci*. 3:904–910.
- Beierlein M, Gibson JR, Connors BW. 2003. Two dynamically distinct inhibitory networks in layer 4 of the neocortex. *J Neurophysiol*. 90:2987–3000.
- Bruno RM, Sakmann B. 2006. Cortex is driven by weak but synchronously active thalamocortical synapses. *Science*. 312:1622–1627.
- Cauli B, Audinat E, Lambolez B, Angulo MC, Ropert N, Tsuzuki K, Hestrin S, Rossier J. 1997. Molecular and physiological diversity of cortical nonpyramidal cells. *J Neurosci*. 17:3894–3906.
- Cauli B, Porter JT, Tsuzuki K, Lambolez B, Rossier J, Quenet B, Audinat E. 2000. Classification of fusiform neocortical interneurons based on unsupervised clustering. *Proc Natl Acad Sci USA*. 97:6144–6149.
- Connors BW, Gutnick MJ. 1990. Intrinsic firing patterns of diverse neocortical neurons. *Trends Neurosci*. 13:99–104.
- Di Cristo G, Wu C, Chattopadhyaya B, Ango F, Knott G, Welker E, Svoboda K, Huang ZJ. 2004. Subcellular domain-restricted GABAergic innervation in primary visual cortex in the absence of sensory and thalamic inputs. *Nat Neurosci*. 7:1184–1186.
- Dotd HU, Zieglgänsberger W. 1990. Visualizing unstained neurons in living brain slices by infrared DIC-videomicroscopy. *Brain Res*. 537:333–336.
- Douglas RJ, Martin KA. 2007. Mapping the matrix: the ways of neocortex. *Neuron*. 56:226–238.
- Dumitriu D, Cossart R, Huang J, Yuste R. 2007. Correlation between axonal morphologies and synaptic input kinetics of interneurons from mouse visual cortex. *Cereb Cortex*. 17:81–91.
- Egger V, Nevian T, Bruno RM. 2008. Subcolumnar dendritic and axonal organization of spiny stellate and star pyramid neurons within a barrel in rat somatosensory cortex. *Cereb Cortex*. 18:876–889.
- Fairén A, DeFelipe J, Regidor J. 1984. Nonpyramidal neurons. In: Peters A, Jones EG, editors. *Cerebral cortex: cellular components of the cerebral cortex*. New York: Plenum Press. p. 206–211.
- Feldman ML, Peters A. 1978. The forms of non-pyramidal neurons in the visual cortex of the rat. *J Comp Neurol*. 179:761–793.
- Feldmeyer D, Egger V, Lübke J, Sakmann B. 1999. Reliable synaptic connections between pairs of excitatory layer 4 neurones within a single 'barrel' of developing rat somatosensory cortex. *J Physiol*. 521:169–190.
- Foehring RC, Lorenzon NM, Herron P, Wilson CJ. 1991. Correlation of physiologically and morphologically identified neuronal types in human association cortex in vitro. *J Neurophysiol*. 66:1825–1837.
- Gibson JR, Beierlein M, Connors BW. 1999. Two networks of electrically coupled inhibitory neurons in neocortex. *Nature*. 402:75–79.
- Gonchar Y, Burkhalter A. 1997. Three distinct families of GABAergic neurons in rat visual cortex. *Cereb Cortex*. 7:347–358.
- Gonchar Y, Wang Q, Burkhalter A. 2008. Multiple distinct subtypes of GABAergic neurons in mouse visual cortex identified by triple immunostaining. *Front Neuroanat*. 1:3. doi:10.3389/neuro.05/003.
- Gupta A, Wang Y, Markram H. 2000. Organizing principles for a diversity of GABAergic interneurons and synapses in the neocortex. *Science*. 287:273–278.
- Helmstaedter M, Sakmann B, Feldmeyer D. 2008a. Neuronal correlates of local, lateral, and translaminar inhibition with reference to cortical columns. *Cereb Cortex*. doi:10.1093/cercor/bhn141.
- Helmstaedter M, Sakmann B, Feldmeyer D. 2008b. L2/3 interneuron groups defined by multi-parameter analysis of axonal projection, dendritic geometry and electrical excitability. *Cereb Cortex*. doi:10.1093/cercor/bhn130.
- Hines ML, Carnevale NT. 1997. The NEURON simulation environment. *Neural Comput*. 9:1179–1209.
- Hirsch JA, Martinez LM, Pillai C, Alonso JM, Wang Q, Sommer FT. 2003. Functionally distinct inhibitory neurons at the first stage of visual cortical processing. *Nat Neurosci*. 6:1300–1308.
- Jonas P, Bischofberger J, Fricker D, Miles R. 2004. Interneuron Diversity series: Fast in, fast out—temporal and spatial signal processing in hippocampal interneurons. *Trends Neurosci*. 27:30–40.
- Jones EG. 1975. Varieties and distribution of non-pyramidal cells in the somatic sensory cortex of the squirrel monkey. *J Comp Neurol*. 160:205–267.
- Jones EG. 1984. Neurogliaform or spiderweb cells. In: Peters A, Jones EG, editors. *Cerebral cortex: cellular components of the cerebral cortex*. New York: Plenum Press. p. 409–418.
- Karube F, Kubota Y, Kawaguchi Y. 2004. Axon branching and synaptic bouton phenotypes in GABAergic nonpyramidal cell subtypes. *J Neurosci*. 24:2853–2865.
- Kawaguchi Y. 1993. Groupings of nonpyramidal and pyramidal cells with specific physiological and morphological characteristics in rat frontal cortex. *J Neurophysiol*. 69:416–431.
- Kawaguchi Y, Kubota Y. 1993. Correlation of physiological subgroupings of nonpyramidal cells with parvalbumin- and calbindinD28k-immunoreactive neurons in layer V of rat frontal cortex. *J Neurophysiol*. 70:387–396.
- Kawaguchi Y, Kubota Y. 1997. GABAergic cell subtypes and their synaptic connections in rat frontal cortex. *Cereb Cortex*. 7:476–486.
- Koch C. 1999. *Biophysics of computation*. Oxford: Oxford University Press.
- Krimer LS, Zaitsev AV, Czanner G, Kroner S, Gonzalez-Burgos G, Povysheva NV, Iyengar S, Barrionuevo G, Lewis DA. 2005. Cluster analysis-based physiological classification and morphological properties of inhibitory neurons in layers 2–3 of monkey dorsolateral prefrontal cortex. *J Neurophysiol*. 94:3009–3022.
- Lorente de No R. 1938. *Cerebral Cortex: Architecture, Intracortical Connections, Motor Projections* (chapter 15). In: Fulton JF, editor. *Physiology of the nervous system*. Oxford: Oxford University Press. p. 288–313.
- Lübke J, Egger V, Sakmann B, Feldmeyer D. 2000. Columnar organization of dendrites and axons of single and synaptically

- coupled excitatory spiny neurons in layer 4 of the rat barrel cortex. *J Neurosci.* 20:5300-5311.
- Mainen ZF, Sejnowski TJ. 1996. Influence of dendritic structure on firing pattern in model neocortical neurons. *Nature.* 382:363-366.
- McBain CJ, Fisahn A. 2001. Interneurons unbound. *Nat Rev Neurosci.* 2:11-23.
- McCormick DA, Connors BW, Lighthall JW, Prince DA. 1985. Comparative electrophysiology of pyramidal and sparsely spiny stellate neurons of the neocortex. *J Neurophysiol.* 54:782-806.
- Miyoshi G, Butt SJ, Takebayashi H, Fishell G. 2007. Physiologically distinct temporal cohorts of cortical interneurons arise from telencephalic Olig2-expressing precursors. *J Neurosci.* 27:7786-7798.
- Nowak LG, Azouz R, Sanchez-Vives MV, Gray CM, McCormick DA. 2003. Electrophysiological classes of cat primary visual cortical neurons in vivo as revealed by quantitative analyses. *J Neurophysiol.* 89:1541-1566.
- Porter JT, Cauli B, Staiger JF, Lambollez B, Rossier J, Audinat E. 1998. Properties of bipolar VIPergic interneurons and their excitation by pyramidal neurons in the rat neocortex. *Eur J Neurosci.* 10:3617-3628.
- Porter JT, Johnson CK, Agmon A. 2001. Diverse types of interneurons generate thalamus-evoked feedforward inhibition in the mouse barrel cortex. *J Neurosci.* 21:2699-2710.
- Rall W. 1959. Branching dendritic trees and motoneuron membrane resistivity. *Exp Neurol.* 1:491-527.
- Ramón y Cajal S. 1904. *Textura del sistema nervioso del hombre y de los vertebrados.* Madrid: Imprenta N. Moya.
- Schaefer AT, Larkum ME, Sakmann B, Roth A. 2003. Coincidence detection in pyramidal neurons is tuned by their dendritic branching pattern. *J Neurophysiol.* 89:3143-3154.
- Somogyi P, Kisvarday ZF, Martin KA, Whitteridge D. 1983. Synaptic connections of morphologically identified and physiologically characterized large basket cells in the striate cortex of cat. *Neuroscience.* 10:261-294.
- Somogyi P, Klausberger T. 2005. Defined types of cortical interneurone structure space and spike timing in the hippocampus. *J Physiol.* 562:9-26.
- Stuart GJ, Dodt HU, Sakmann B. 1993. Patch-clamp recordings from the soma and dendrites of neurons in brain slices using infrared video microscopy. *Pflugers Arch.* 423:511-518.
- Szentagothai J. 1973. Synaptology of the visual cortex. In: Jung R, editor. *Handbook of sensory physiology.* New York: Springer-Verlag. p. 269-324.
- Tamás G, Somogyi P, Buhl EH. 1998. Differentially interconnected networks of GABAergic interneurons in the visual cortex of the cat. *J Neurosci.* 18:4255-4270.
- Toledo-Rodriguez M, Goodman P, Illic M, Wu C, Markram H. 2005. Neuropeptide and calcium-binding protein gene expression profiles predict neuronal anatomical type in the juvenile rat. *J Physiol.* 567:401-413.
- Wang Y, Gupta A, Toledo-Rodriguez M, Wu CZ, Markram H. 2002. Anatomical, physiological, molecular and circuit properties of nest basket cells in the developing somatosensory cortex. *Cereb Cortex.* 12:395-410.
- Ward JH. 1963. Hierarchical grouping to optimize an objective function. *J Am Stat Assoc.* 58:236-244.
- Whittington MA, Traub RD. 2003. Interneuron diversity series: inhibitory interneurons and network oscillations in vitro. *Trends Neurosci.* 26:676-682.
- Zaitsev AV, Gonzalez-Burgos G, Povysheva NV, Kroner S, Lewis DA, Krimer LS. 2005. Localization of calcium-binding proteins in physiologically and morphologically characterized interneurons of monkey dorsolateral prefrontal cortex. *Cereb Cortex.* 15: 1178-1186.